CRYSTAL GROWTH & DESIGN

Article

Polymorphism in the anti-inflammatory drug Flunixin and its relationship with Clonixin.

María Cecilia Dávila-Miliani, Analio Dugarte-Dugarte, Robert A. Toro, Jines E. Contreras, Hernando A. Camargo, Jose Antonio Henao, José Miguel Delgado, and Graciela Díaz de Delgado

Cryst. Growth Des., **Just Accepted Manuscript** • DOI: 10.1021/acs.cgd.0c00284 • Publication Date (Web): 14 May 2020

Polymorphism in the anti-inflammatory drug Flunixin and its relationship with Clonixin.

María Cecilia Dávila-Miliani[1], Analio Dugarte-Dugarte[1], Robert A. Toro[2], Jines E. Contreras[1], Hernando A. Camargo[3], José Antonio Henao[2], José Miguel Delgado[1], Graciela Díaz de Delgado[1]

[1]Laboratorio de Cristalografía-LNDRX, Departamento de Química, Facultad de Ciencias, Universidad de los Andes, Mérida 5101, Venezuela.
[2]Grupo de Investigación en Química Estructural (GIQUE), Escuela de Química, Universidad Industrial de Santander, Bucaramanga, Colombia.
[3]Grupo de Investigación en Nuevos Materiales y Energías Alternativas, Facultad de Química Ambiental, Universidad Santo Tomás, Florida Blanca, Colombia.
email: diaz@ula.ve / gdiazdedelgado@gmail.com

ABSTRACT

Crystallization of the NSAID flunixin in acetone and in acetone-hexane produced two conformational polymorphs, as predicted by hydrogen bond propensity analyses, which are similar to three of the polymorphs of the related NSAID clonixin. The two polymorphs of flunixin display an intramolecular hydrogen bond between the amine N—H and the carbonyl oxygen of the carboxylic group. However, the intermolecular hydrogen bond pattern of Form I (crystallized from acetone) is characterized by the acid—pyridine heterosynthon while Form II (from acetone-hexane) displays the acid—acid homosynthon. Form I of flunixin is similar to form I of clonixin while form II of flunixin is related to forms III and IV of clonixin. Hirshfeld surface maps were used to show the differences in the interactions present in the two flunixin polymorphs and the similarities with the polymorphs of the related compound clonixin. Energy framework calculations corroborate the similarity between Form I of flunixin and clonixin and indicate that Form II of flunixin is more closely related to Form IV of clonixin than to Form III.

Keywords: Flunixin, Clonixin, NSAID, polymorphism, hydrogen bond propensity, Hirshfeld surfaces, energy frameworks.

INTRODUCTION

Non-steroidal anti-inflammatory drugs (NSAIDs) comprise a heterogeneous family of compounds which inhibit the prostaglandin G/H synthase enzymes (or cyclooxygenases) involved in painful and inflammatory responses to a variety of stimuli. Selective pain and inflammation relief by NSAIDs is thought to be related to inhibition of Cyclooxygenase-2 (COX-2) while COX-1 inhibition is usually related to the adverse effects of such drugs.[1] An important class of non-narcotic NSAIDs are diarylamine derivatives containing a carboxylic acid group. They can also be regarded as derivatives of phenylacetic and nicotinic acids. Diclofenac, mefenamic acid, tolfenamic acid, niflumic acid, belong to this group of compounds.[1] In particular diclofenac is among the top 200 most prescribed drugs, with more than 9.5 million prescriptions in 2015 in the US.[2] Other compounds of this group, such as clonixin (**3**, figure 1) in the form of its lysine salt, have shown improved analgesic activity. The development and use of clonixin led to the discovery and study of the closely related compound flunixin (**1**, figure 1) which is presented in this contribution.

Flunixin is usually formulated as its meglumine salt[3] where meglumine (**2**, figure 1) can be considered as an excipient which increases the solubility of flunixin.[4] Some commonly used brand names are *Banamine*®, *Flumeglumine®, Suppressor*®, *Binixin®, and Finadyne*®. It is frequently used in veterinary medicine, including food-producing animals, in contrast to clonixin which is prescribed only for human consumption. Flunixin is widely administered to horses to alleviate muscle pain, colic pain, and in the treatment of joint diseases. It is considered a controlled substance in equestrian sports and, therefore, its use is under strict regulation.[5] The analgesic action of flunixin involves the same mechanism as the other NSAIDs, blocking pain impulse generation by inhibiting the enzyme cyclooxygenase and causing a decrease in the synthesis of prostaglandins.[3,6] The crystal structure of the flunixin-meglumine salt has been previously reported,[4] but searches in the Cambridge Structural Database (CSD)[7] and the PDF-4/Organics database[8] indicated that the structure of flunixin is not known.

Many diarylamines and drugs belonging to this family exhibit polymorphism.[9-16] Given the close relationship between flunixin and clonixin, a screening was carried out to explore the possibility of polymorphism in flunixin. For clonixin four polymorphs have been identified.[17] Forms I, III,

and IV are neutral, while form II is zwitterionic (Figure 2). It is one of the few molecules in the CSD that has zwitterionic polymorphs.[15] In forms I and II the molecules form carboxylic-pyridine hydrogen bonds (hetero-synthons) while in forms III and IV they display carboxylic acid dimers (homo-synthons). The conformation of the molecules is different in each polymorph.

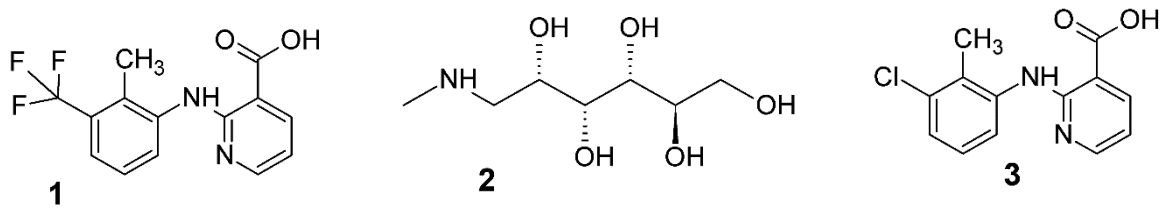

Figure 1. Molecular diagrams of flunixin (**1**), meglumine (**2**), and clonixin (**3**).

In view of the polymorphism exhibited by clonixin, the possible formation of polymorphs of flunixin was examined experimentally, by performing crystallization experiments, and by using the Hydrogen Bond Propensity tool included in the CSD-Materials suite implemented in Mercury[18], comparing with the calculation for the polymorphs of clonixin. This tool, based on statistical considerations, has proven to be of great value in the study, prediction, and rationalization of polymorphism of many pharmaceutical compounds as well as to assess the potential formation of multicomponent materials.[19-21]

As part of the work being carried out in our laboratories on the structural characterization of active pharmaceutical ingredients (APIs) and their metal derivatives, the characterization by Attenuated Total Reflectance Infrared Spectroscopy (ATR-FTIR), Thermogravimetric analysis (TGA), Differential Scanning Calorimetry (DSC), and powder and single crystal X-ray diffraction (PXRD and SCXRD), of two polymorphs of flunixin (obtained so far) is reported in the present work. Hydrogen Bond Propensity studies, Hirshfeld surface analysis, and Energy frameworks calculations are also presented.

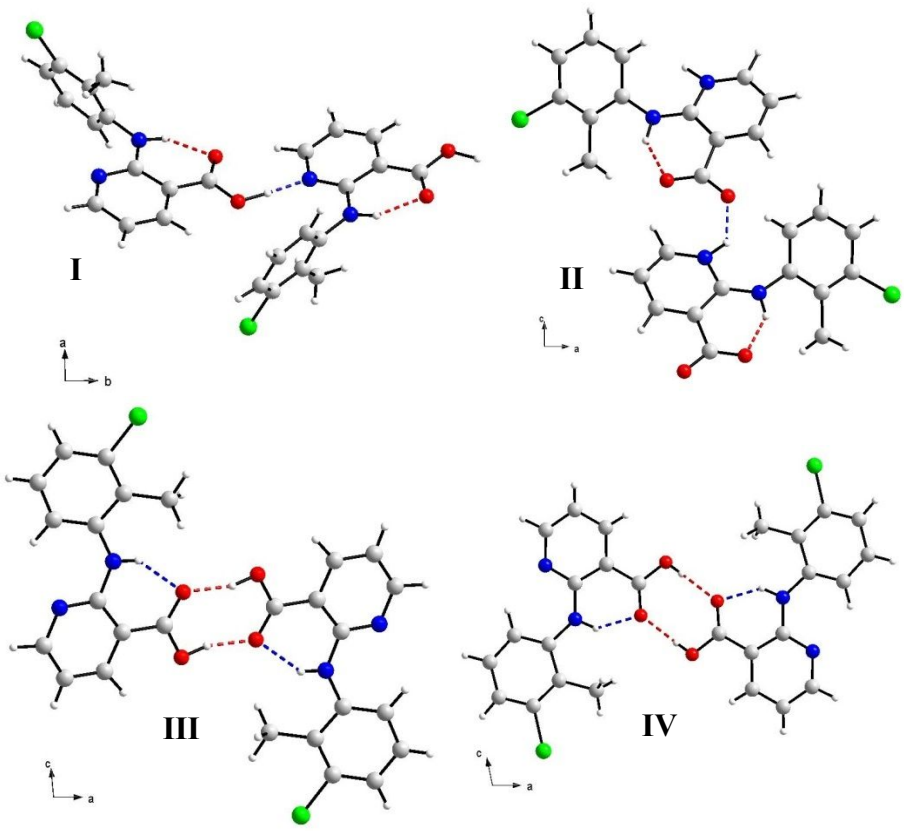

Figure 2. Hydrogen bonds present in the four polymorphs of clonixin. Figures drawn using the data included in the corresponding CSD entries (I; BIXGIY, II: BIXGIY04, III: BIXGIY02, IV: BIXGIY03).

RESULTS AND DISCUSSION

1. Crystallization experiments

Flunixin was separated from flunixin-meglumine raw material (FM-RM) as described in the Experimental section. Crystallization in acetone solution of the precipitated flunixin (FP) produced the colorless prisms of Form I shown in Figure SI-1a of the Supporting Information file. On the other hand, crystallization in acetone/hexane produced needles of Form II (Figure SI-1b) as well as prismatic crystals of Form I.

2. Infrared spectroscopy and thermal analysis

The ATR-FTIR spectra of flunixin-meglumine raw material (FM-RM), flunixin precipitated (FP), and Form I of flunixin (F-I) are shown in Figure SI-2. The characteristic bands of the functional groups present in the molecules are observed as summarized in Table SI-1. The infrared spectrum of FM-RM (Figure SI-2a) shows the N-H stretching vibration of the secondary amine group of the flunixin moiety at 3359 cm^{-1} and the N-H stretching vibrations of the protonated amine of meglumine between 2842 and 2915 cm^{-1}, overlapped with the C_{sp3}–H and C_{sp2}–H stretching vibrations. The multiple hydrogen-bonded hydroxyl groups present in the meglumine moiety produce a broad band centered around 3150 cm^{-1}. The two bands at 1584 cm^{-1} and 1370 cm^{-1} correspond to the asymmetric and symmetric stretching vibrations of the carboxylate group of flunixin. The C=C stretching bands of flunixin are observed at 1601 cm^{-1}. For FP and F-I (Figures SI-2b and SI-2c) the N-H stretch is observed at 3237 and 3236 cm^{-1}, respectively. The stretching band of the carboxylic O–H is very broad and weak. The C=O stretch appears between 1673 cm^{-1} and 1672 cm^{-1}. The absorption bands due to the φ–N and N–py stretches are observed at 1316 and 1239 cm^{-1}, respectively, while the stretching vibrations of the C=N and C=C bonds appear as two overlapped bands at 1599-1580 cm^{-1}. The overtones of the O–H bending are expected to overlap with the asymmetric and symmetric vibrations of the methyl C–H bonds between 2900 and 2200 cm^{-1}, while the O-H bending vibration is observed at 1452-1451 cm^{-1}. In the two spectra, the characteristic absorption bands of the trifluoromethyl group are observed in the range 1141-1120 cm^{-1}.

The thermogram for flunixin recrystallized in acetone (Form I, Figure SI-3a) shows stability up to approximately 200 °C when melting and decomposition start to occur. The total weight loss is 94.7 %. The DSC shows a sharp endotherm at 235.0 °C associated to melting. A broad endotherm at 277.1 °C and a sharp endotherm at 283.3 °C are associated to decomposition. The TGA/DSC of Flunixin recrystallized in acetone/hexane, from which Form-II was identified, showed the same thermal behavior observed for Form I (Figure SI-3b). This may be the result of the presence of an important amount of Form I in the sample, as mentioned before. For comparison, the TGA/DSC of flunixin-meglumine raw material (FM-RM) is presented in Figure SI-3c. FM-RM shows stability up to 258 °C when a two-step weight loss of 85.52%, with peak temperatures 288 and 350 °C is observed. The DSC shows an endothermic transition without weight loss with peak temperature of 142.0 °C that corresponds to melting. The TGA/DSC of Flunixin powder (Figure SI-3d) shows

melting at 230.9 °C and the endotherm associated with decomposition is observed at 267.9 °C. An endothermic event at 171.4 °C is observed which has not been possible to correlate to known phases in the system. It is being investigated and any results will be reported elsewhere.

3. X-ray diffraction

Structure determination and refinement from powder diffraction data of Form I.

The excellent quality of the powder diffraction pattern obtained for Flunixin precipitated from flunixin-meglumine raw material (FM-RM) as described in the Experimental section, allowed us to successfully determine the structure from powder data. The details of the structure determination and refinement from powder data are presented in the Supporting Information file, Section SI-3, Figure SI-4 and Tables SI-2a,b,c.

Structure determination and refinement from single crystal data

Table 1 summarizes the crystal data, experimental conditions, and final refinement parameters for the studies at ambient temperature (RT) and low temperature (LT) of flunixin Form I, and at ambient temperature of Form II. A low temperature study of the needles of Form II was not possible due to the small amount obtained and their low crystal quality. Section SI-4 of the Supporting Information contains tables of atomic coordinates, anisotropic displacement parameters for non-hydrogen atoms, and isotropic displacement parameters for hydrogen atoms (Tables SI-3a,b,c) for Form I-RT, Form I-LT, and Form II-RT. Corresponding bond lengths and angles are presented in Tables SI-4a,b,c and Table SI-5 summarizes the calculated geometric parameters for hydrogen bonds and intermolecular contacts for the two polymorphs of flunixin.

Table 1. Crystal data, experimental conditions, and refinement results for flunixin Form I (ambient and low temperature) and Form II (ambient temperature).

	Form I (Amb. temperature)	**Form I (Low temperature)**	**Form II**
Formula	$C_{14}H_{11}F_3N_2O_2$	$C_{14}H_{11}F_3N_2O_2$	$C_{14}H_{11}F_3N_2O_2$
Formula Weight	296.25	296.25	296.25
Crystal System	monoclinic	monoclinic	triclinic
Space group	$P2_1/c$ (No. 14)	$P2_1/c$ (No. 14)	$P\bar{1}$ (No. 2)
Unit cell parameters	***a*** = 7.6842(3) Å ***b*** = 14.1394(5) Å ***c*** = 12.5115(5) Å β = 102.138(4)°	***a*** = 7.580(14) Å ***b*** = 14.14(3) Å ***c*** = 12.45(2) Å β = 102.32(2)°	***a*** = 7.3684(5) Å ***b*** = 7.6617(5) Å ***c*** = 11.7865(8) Å α = 79.684(5)° β = 85.082(6)° γ = 87.191(6)°
V (Å^3)	1328.98(9)	1304(4)	651.85(8)
Z	4	4	2
D(calc) (g cm^{-3})	1.481	1.509	1.509
μ(MoKα) (mm^{-1})	0.128	0.131	0.131
Crystal Size (mm)	0.23 x 0.44 x 0.46	0.09 x 0.10 x 0.22	0.03 x 0.08 x 0.23
Temperature (K)	293	100	293
Radiation, λ (Å)	MoKα, 0.71073	MoKα, 0.71073	MoKα, 0.71073
θ Min-Max (°)	3.6, 27.4	2.2, 32.3	2.8, 28.2
Limiting indices	$-9 \le h \le 9$ $-18 \le k \le 18$ $-16 \le l \le 15$	$-4 \le h \le 10$ $-13 \le k \le 19$ $-18 \le l \le 3$	$-9 \le h \le 8$ $-9 \le k \le 10$ $-14 \le l \le 15$
Tot., Uniq. Data, R_{int}	11671, 2939, 0.023	3642, 2717, 0.057	10000, 2681, 0.062
Obs. Data (I > 2.0 σ(I))	2407	1441	1576
Nref, Npar	2939, 197	2717, 197	2681, 197
R, wR_2, S	0.0432, 0.1255, 1.03	0.0394, 0.0716, 0.75	0.0551, 0.1618, 0.96
Min. and Max. Resd. Dens. (e$^-$ Å^{-3})	-0.22, 0.19	-0.22, 0.26	-0.19, 0.18

Crystal structure of Form I

During the course of the Rietveld refinement of the structure of flunixin (FP) obtained by separation from the flunixin-meglumine raw material, colorless prismatic crystals of appropriate size and quality for single crystal studies were obtained from an acetone solution. The analysis of the single

crystal data indicated that the structure of these crystals is the same as the structure determined from powder data. This phase was assigned as Form I of flunixin, which crystallizes in a monoclinic unit cell with space group $P2_1/c$ and unit cell parameters $\boldsymbol{a}$ = 12.484(2) Å, $\boldsymbol{b}$ = 14.126(3) Å, $\boldsymbol{c}$ = 7.682(2) Å, β = 102.01(1)°, V = 1327.58(3) Å^3, Z = 4. It is worth noting that bond distances and angles from the powder diffraction study are in the range suggested in the statistical analysis performed with Mogul Geometry Check[22] and agree with the results from the single crystal data. The following discussion of the structure of Form I will use the results from the single crystal data.

The asymmetric unit contains one flunixin molecule (Figure 3a) in which the pyridine ring forms a 71.12(7)° angle with the plane of the substituted phenyl ring. The superposition of the molecules of flunixin in Form I obtained in the powder diffraction study and in the single crystal studies at ambient and low temperature shows that the conformations are the same (Figure 3b) and indicates the good quality of the structure determination from powder diffraction data. The torsion angle C5-N2-C6-C7 is 111.8(2)° at 293 K and 113.7(2)° at 100 K.

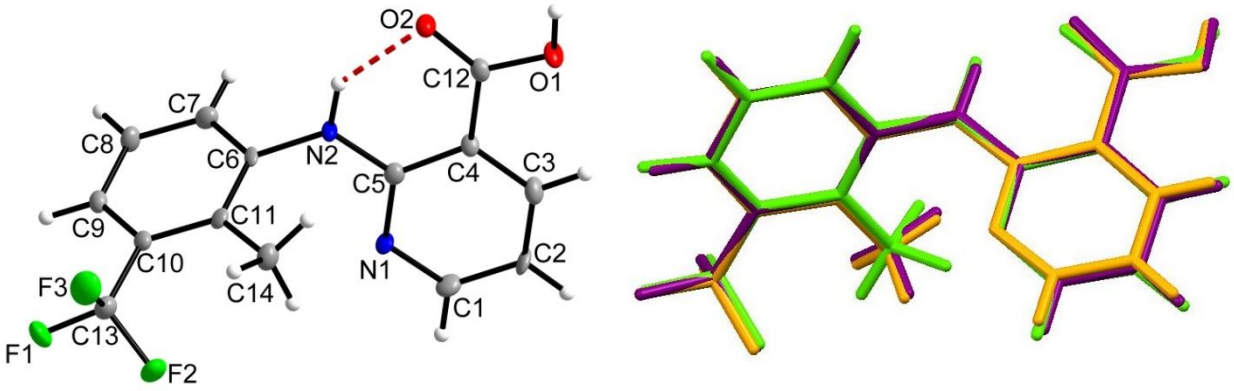

(a) (b)

Figure 3. (a) Molecular structure of flunixin form I (from the low temperature study). Ellipsoids drawn at the 50% level of probability. (b) Superposition of the flunixin molecules in Form I obtained from powder diffraction (green), ambient temperature (orange), and low temperature (purple) studies.

The packing of flunixin molecules in form I is shown in Figure 4. There is one intramolecular hydrogen bond [N2—H2A···O2] represented by the graph set symbol S(6).[23] The molecules

interact by carboxylic-pyridine O1—H1A···N1 and C1—H1···O2 hydrogen bonds to form chains that alternate directions along the **+b** and **-b** axis. This hetero-synthon produces a ring which can be described by the symbol $R_2^2(7)$. The same C1—H1 donor participates in a bifurcated hydrogen bond with one fluorine atom [C1—H1···F2] connecting the chains in a zigzag fashion. Additionally, π···π interactions between the phenyl rings build up a bidimensional network approximately parallel to the **ab**-plane (Figure 4a). These layers are further connected *via* weaker π···π interactions between the pyridine rings along the **c**-axis (Figure 4b). Hydrogen bonds and π···π contacts, calculated with PLATON,[24] are summarized in Table SI-5 in the Supporting Information.

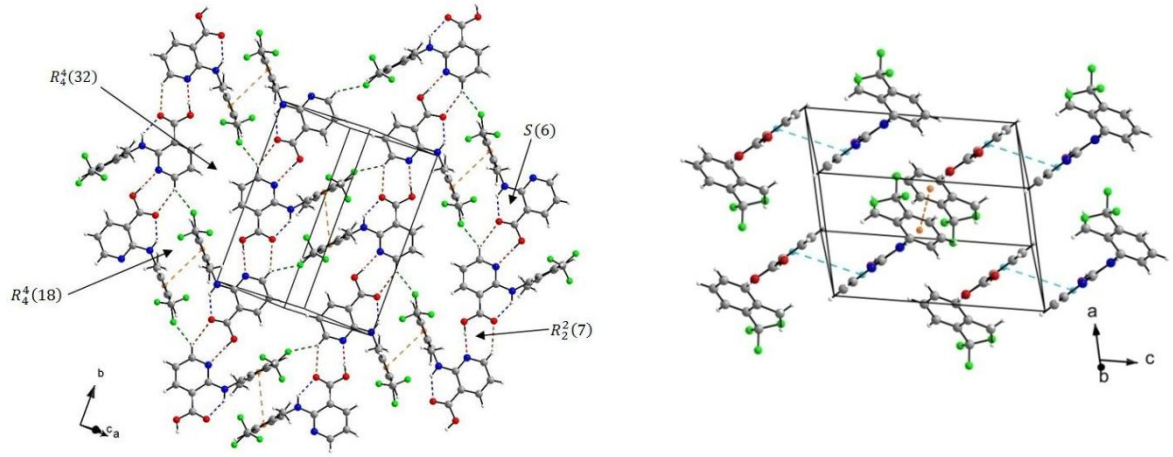

(a) (b)

Figure 4. Two views of the structure of Form I of flunixin. (**a**) Hydrogen bonds and π···π interactions which produce layers parallel to the **ab**-plane. (**b**) Detail of the π···π interactions which connect the layers along the **c**-axis.

Crystal structure of Form II

Flunixin Form II crystallizes in the triclinic system, space group $P\bar{1}$, with parameters ***a*** = 7.3700(5) Å, ***b*** = 7.6640(5) Å, ***c*** = 11.7894(7) Å, α = 79.687(5)°, β = 85.089(5)°, γ = 87.190(5)°, V = 652.36(7) Å^3, Z = 2. The asymmetric unit also contains one flunixin molecule but, in contrast to Form I, the molecules adopt a planar conformation (Figure 5a). The C5-N2-C6-C7 torsion angle is

2.2(4)°, in contrast with the torsions displayed by the flunixin molecule in Form I. The superposition of the molecules in Forms I and II is shown in Figure 5b.

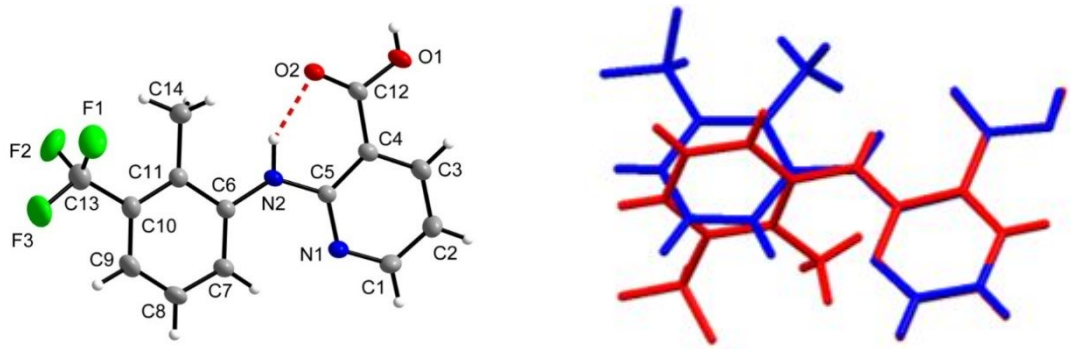

(a) (b)

Figure 5. (a) Molecular structure of flunixin form II. Ellipsoids drawn at the 30% level of probability. (b) Superposition of the molecules in form I (red) and form II (blue).

The packing in form II is shown in Figure 6. There is one intramolecular hydrogen bond as in form I, N2—H2A···O2, represented by the graph set symbol S(6). The molecules interact *via* the carboxylic acid – carboxylic acid homosynthon O1—H1A···O2, which is represented by the symbol $R_2^2(8)$, forming dimers which connect through C3—H3···F3 hydrogen bonds to produce ribbons parallel to the **bc** plane (Figure 6a). The ribbons stack in an alternating fashion at an angle of 18.82° from the ***a***-axis, by means of C14—H14C····π interactions between the methyl group of a phenyl ring and a pyridine ring related by the symmetry operation 1-*x*, 1-*y*, 1-*z* as depicted in Figure 6b. Additionally, there are π····π interactions between these rings. As mentioned before, the geometric parameters for these interactions are summarized in Table SI-5.

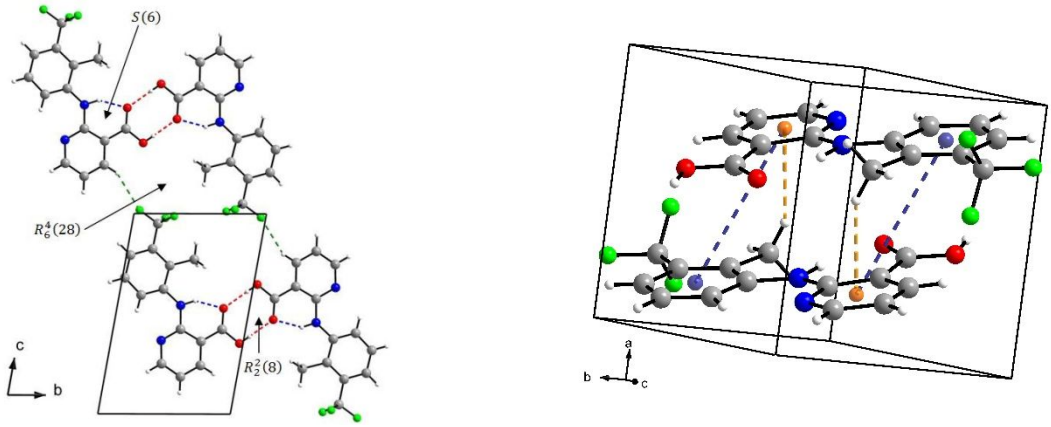

(a) (b)

Figure 6. Two views of the structure of form II of flunixin. (**a**) Cyclic O—H···O hydrogen bonds and C—H···F interactions which produce ribbons parallel to the **bc**-plane. (**b**) C—H····π and π····π interactions which connect ribbons approximately along the **a**-axis.

For comparison purposes, the experimental powder diffraction pattern for flunixin Form I is presented along with the calculated patterns from single crystal data for Form I and Form II (Figure SI-5). As can be seen, the calculated diffraction pattern of Form I coincides with the recorded pattern of the precipitated flunixin powder.

4. Hydrogen bonding propensity analysis

Given the close relationship between flunixin (**1**) and clonixin (**3**), and the report of four polymorphs for the latter, it was considered of interest to carry out a hydrogen bond propensity (HBP) analysis with Mercury.[18,20-21] Section SI-5 of the Supporting Information summarizes de details of the calculations. Figure SI-6 shows the selected hydrogen bond donors and acceptors. The results of the calculations are presented in Table 2.

Table 2. Predicted and Realized Intermolecular Hydrogen Bonds for polymorphs I and II of Flunixin and I, II, III, and IV of Clonixin

Flunixin Forms I and II				Clonixin Forms I, III, IV				Clonixin Form II			
D	**A**	**P**	**Obs.**	**D**	**A**	**P**	**Obs.**	**D**	**A**	**P**	**Obs.**
O1—H	N1	0.45	Form I	O1—H	N1	0.42	Form I	N1—H	O1	0.74	Form II
O1—H	O2	0.41	Form II	O1—H	O2	0.36	Forms III and IV	N1—H	O2	0.74	
N2—H	N1	0.25		N2—H	N1	0.23		N2—H	O1	0.65	
N2—H	O2	0.22		N2—H	O2	0.19		N2—H	O2	0.65	
O1—H	F1	0.06		O1—H	O1	0.03		N1—H	Cl1	0.01	
O1—H	F2	0.06		O1—H	Cl1	0.02		N2—H	Cl1	0.01	
O1—H	F3	0.06		N2—H	O1	0.01		N1—H	N2	0.00	
O1—H	O1—H	0.06		N2—H	Cl1	0.01		N2—H	N2	0.00	
N2—H	F1	0.03		O1—H	N2	0.00					
N2—H	F2	0.03		N2—H	N2	0.00					
N2—H	F3	0.03									

D: Donor; A: Acceptor; P: Propensity.

For all polymorphs of flunixin and clonixin, the calculations indicate an intramolecular hydrogen bond with the highest propensity involving the N2 from the secondary amine and a carboxylate oxygen O2 (N2—H···O2). This intramolecular hydrogen bond is, indeed, present in the two polymorphs of flunixin and the four polymorphs of clonixin.

Regarding the intermolecular hydrogen bonds, the highest propensities calculated involve the carboxylic acid-pyridine hydrogen bond O1—H···N1, as shown in Table 2. This interaction is present in forms I of flunixin and of clonixin. The second highest propensities are for the carboxylic acid dimer O1—H···O2, which is present in flunixin form II and clonixin forms III and IV. For polymorph II of clonixin (zwitterionic) the HBP analysis correctly predicts the intermolecular hydrogen bond between the pyridine N1—H and the carboxylate oxygens present in this structure (N1—H···O1).

Figure SI-7 is the putative landscape for flunixin and shows that the two polymorphs obtained fall in the highest propensity zone. Based on these calculations, it should also be possible to obtain other polymorphs of flunixin, as is observed for clonixin and other related compounds. This possibility is currently under investigation. Interestingly, for the related NSAID niflumic acid,

which differs from flunixin in the absence of the methyl group next to the $-CF_3$ in the phenyl group, only one crystal form has been reported.[25]

5. Hirshfeld surface analysis.

Hirshfeld surface analysis has recently gained attention for the description of intermolecular close contacts since "fingerprint plots" of d_e/d_i interactions are particularly useful in assessing differences in the contact environment of molecules in polymorphs.[26] These fingerprint plots, calculated with CrystalExplorer17,[27] are shown in Figure 7 for polymorph I of flunixin and in Figure 8 for polymorph II.

From Figure 7, the dominant interaction in polymorph I corresponds to the H···N hydrogen bonds, followed by H···O, H···F, and H···C interactions. Weaker interactions such as π···π contacts are present but do not contribute significantly to the fingerprint plot. The fingerprint plot for polymorph II (Figure 8) is very different from the plot for polymorph I. In this case, the dominant interaction is the O—H···O cyclic hydrogen bond. H···F and H···C interactions are also important. The contribution of π····π interactions is more important in polymorph II than in polymorph I. Figure 9 summarizes the percentage contribution of important intermolecular contacts to the Hirshfeld surface area for the two polymorphs of flunixin.

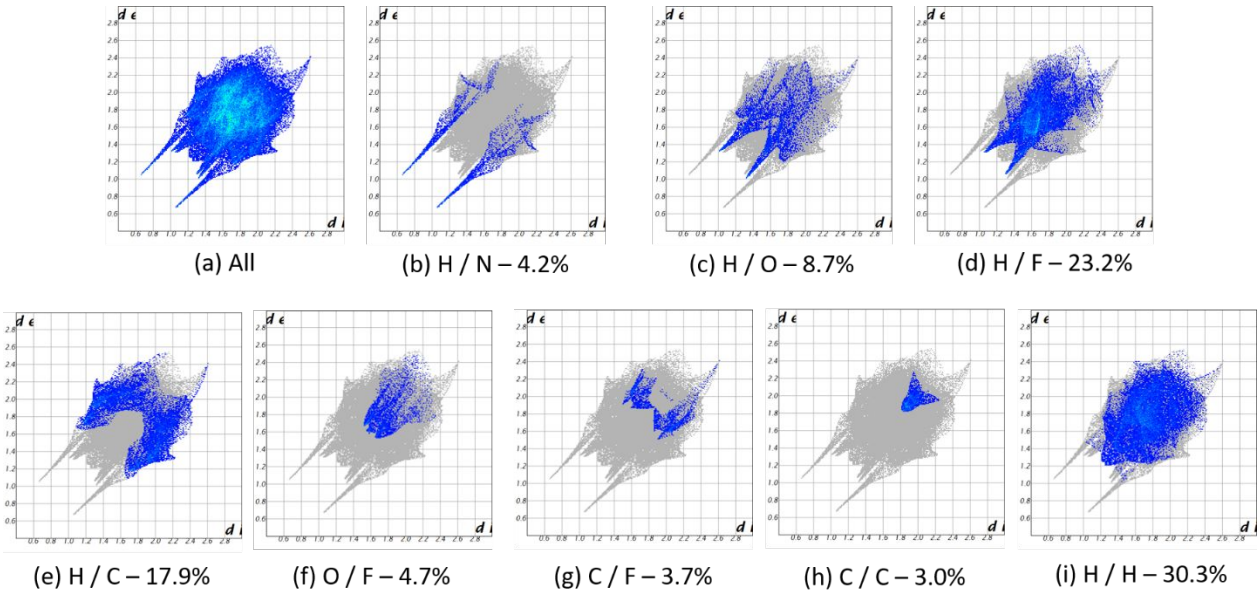

Figure 7. Fingerprint plots for the molecule of flunixin Form I. (a) all contacts; (b) H···N contacts; (c) H···O contacts; (d) H···F contacts; (e) H···C contacts; (f) O···F contacts; (g) C···F contacts; (h) C···C contacts; (i) H···H contacts. The percent of surface area included is shown for each plot.

Fingerprint plots were also calculated for the four polymorphs of clonixin and are included in Figures SI-8 to SI-11 of the Supporting Information file. Figure 10 shows the fingerprint plots including all contacts for the two polymorphs of flunixin and the four polymorphs of clonixin. It is worth noting the resemblance of the plots for flunixin form I and clonixin form I and between form II of flunixin and forms III and IV of clonixin. A summary of the contribution of intermolecular interactions to the Hirshfeld surface in terms of percentage surface area is presented in Figure SI-12.

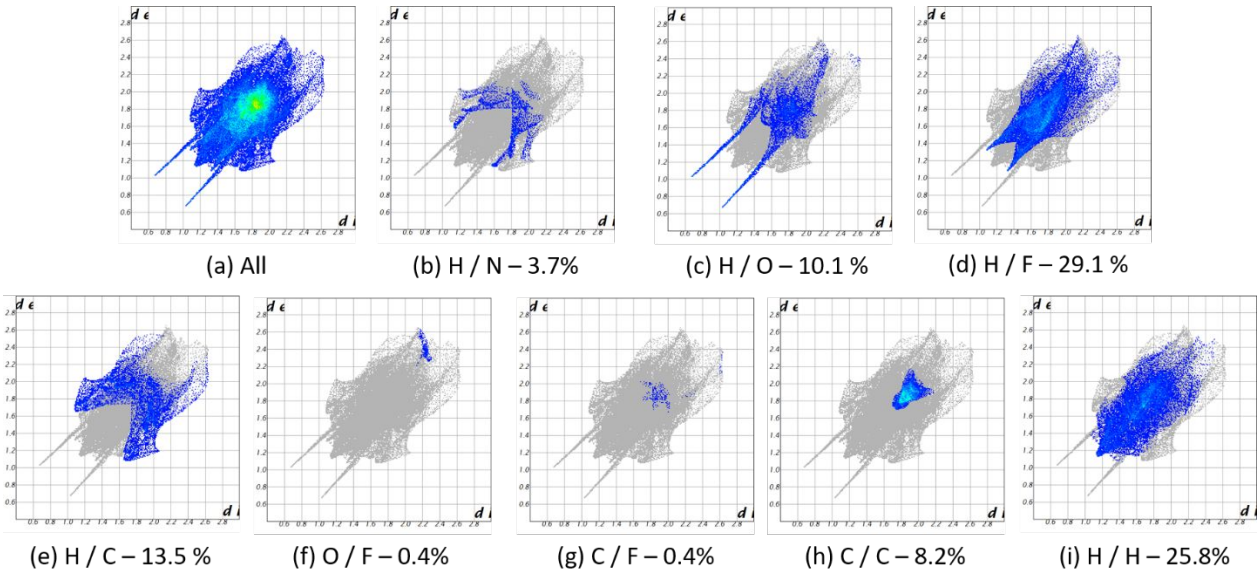

Figure 8. Fingerprint plots for the molecule of flunixin Form II. (a) all contacts; (b) H···N contacts; (c) H···O contacts; (d) H···F contacts; (e) H···C contacts; (f) O···F contacts; (g) C···F contacts; (h) C···C contacts; (i) H···H contacts. The percent of surface area included is shown for each plot.

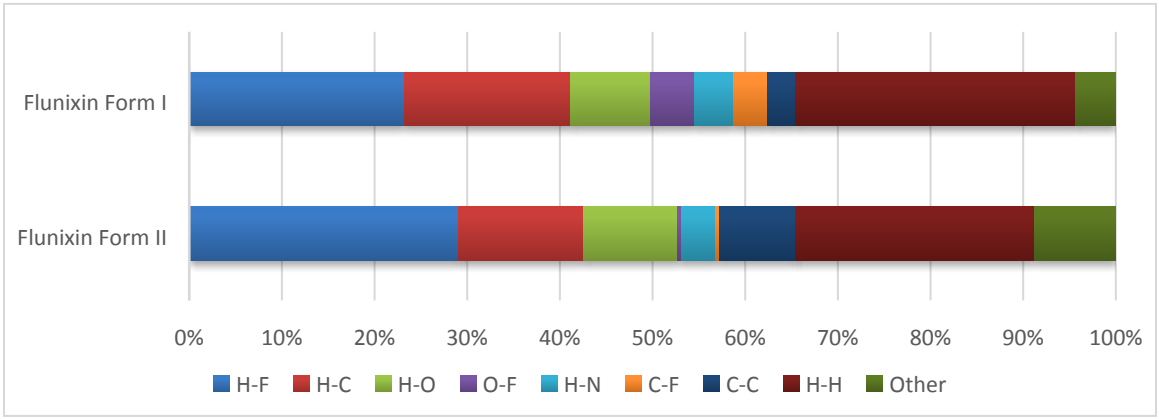

Figure 9. Contribution of important intermolecular contacts (%) to the Hirshfeld surface area for the two polymorphs of flunixin.

Additionally, the d_{norm} parameter mapped onto the Hirshfeld surface allows to better visualize contacts shorter than the sum of van der Waals radii. Figure 11 shows d_{norm} mapped for both polymorphs of flunixin. In form I, the strongest red area (shortest contact) corresponds to the O—H···N hydrogen bond, shown on both sides of the molecule (the carboxylic group and the pyridine

ring) while smaller red areas are related to weaker C—H···O and C—H···F interactions. In form II, the cyclic O—H···O hydrogen bond corresponds to the strongest red spots because it is the strongest interaction in the structure, even stronger than the O—H···N hydrogen bond in polymorph I. A small red spot related to the C—H···F interaction is also observed in the map of form II.

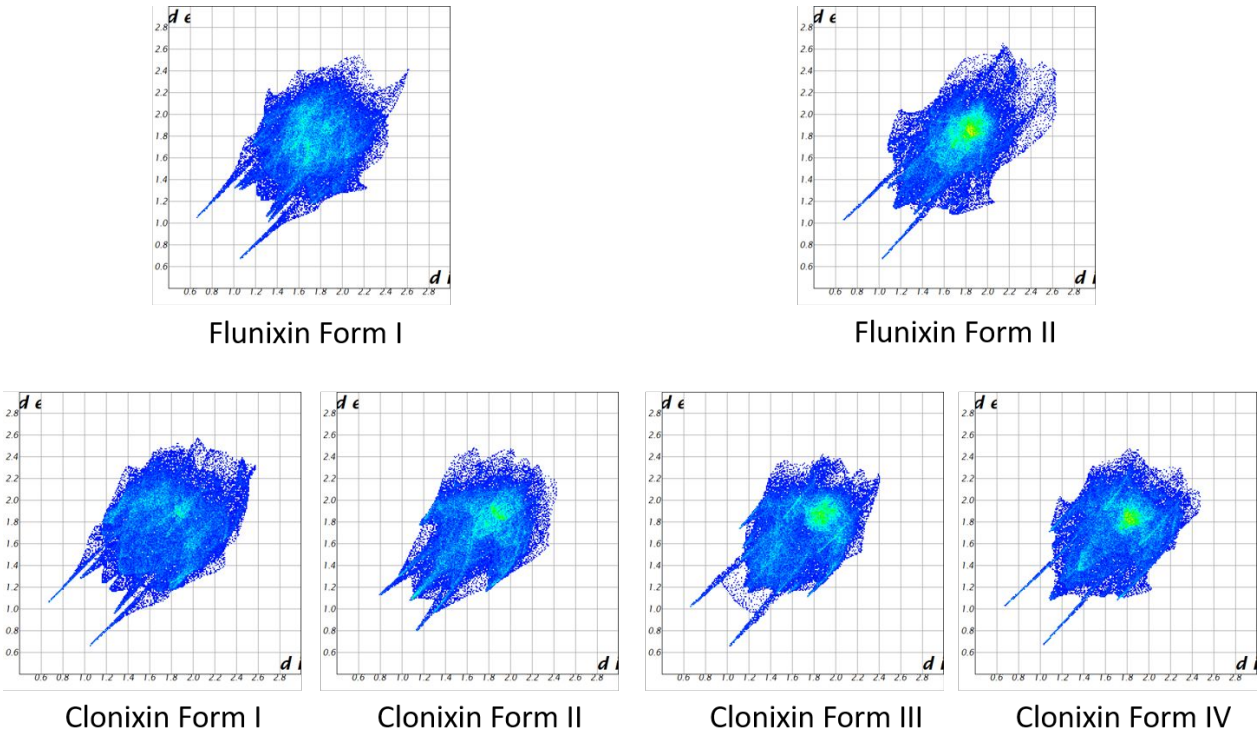

Figure 10. Fingerprint plots calculated for all contacts in the two polymorphs of flunixin and the four polymorphs of clonixin.

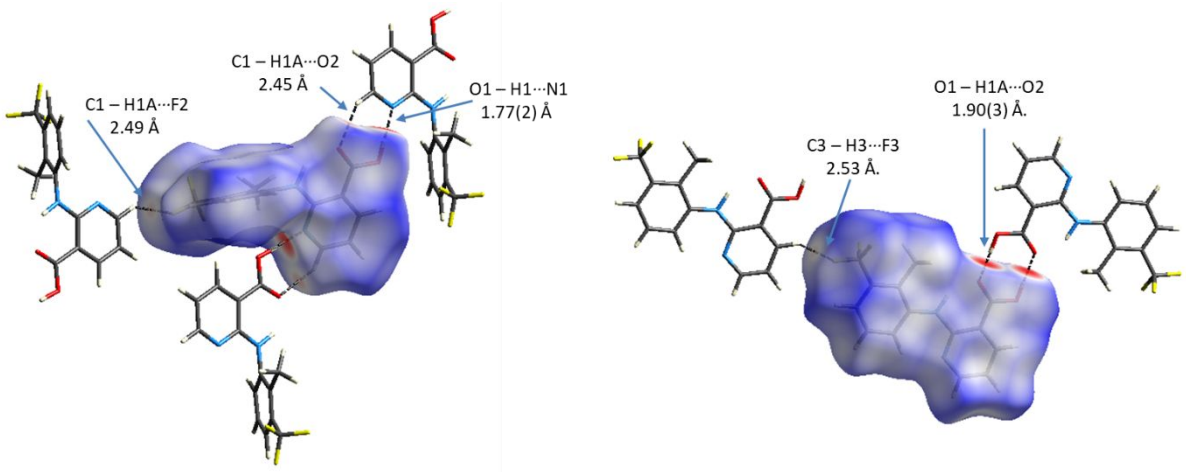

(a) (b)

Figure 11. Mapping of the d_{norm} parameter in the range -0.70 to 1.32 onto the Hirshfeld surface for (a) Form I and (b) Form II of flunixin. The strongest close contacts with neighboring molecules are shown for each polymorph.

6. Energy framework analysis.

Figures 12 and 13 contain a representation, in 2x2x2 unit cells, of the electrostatic, dispersion, and total energy for the polymorphs of flunixin and clonixin. Table 3 presents a summary of the contributions to the total energy of the individual energy components for these polymorphs. The complete results of the calculations are presented in Tables SI-8 to SI-13 of the Supporting Information.

As it was discussed in previous sections, polymorphs I of flunixin and of clonixin display the same molecular configuration, hydrogen bonding pattern, and a similar distribution of intermolecular interactions as seen in the calculated fingerprint plots. Similarly, polymorph II of flunixin shares those same features with polymorphs III and IV of clonixin. The calculations of energy frameworks for all polymorphs support those findings. A comparison with clonixin Form II is not appropriate because of the zwitterionic nature of the clonixin fragment in this polymorph.

As seen in Figure 12, forms I of flunixin and of clonixin show the same topology for the contributions of the electrostatic and dispersive energies to the total energy of interactions. The values for the individual contributions are also similar (Table 3) leading to similar values of E_{tot}. On the other hand, a comparison of the energy framework for polymorph II of flunixin (F-II) with clonixin polymorphs III and IV (C-III and C-IV) indicates a closest resemblance of F-II to C-IV (Figure 13). Fingerprint plots pointed to similarities in intermolecular contacts between F-II, C-III, and C-IV, but energy frameworks calculations provide a better insight into the contributions to the total interaction energy which allows to identify a closer resemblance between F-II and C-IV.

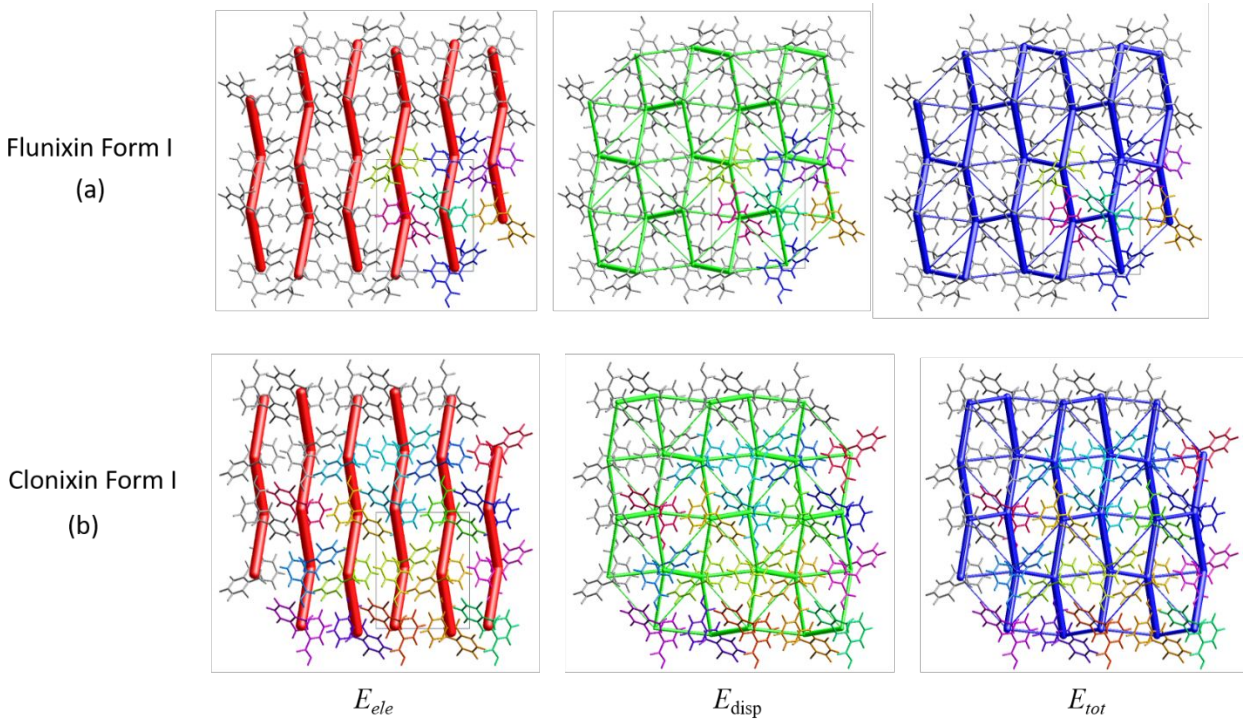

Figure 12. Energy frameworks viewed down the ***a*-**axis for (a) Flunixin Form I and (b) Clonixin Form I. The cylinder radii was scaled to 75 arbitrary units and the energy cutoff is 5 kJ mol^{-1}. E_{ele}, E_{disp}, and E_{tot} are represented in red, green, and blue, respectively.

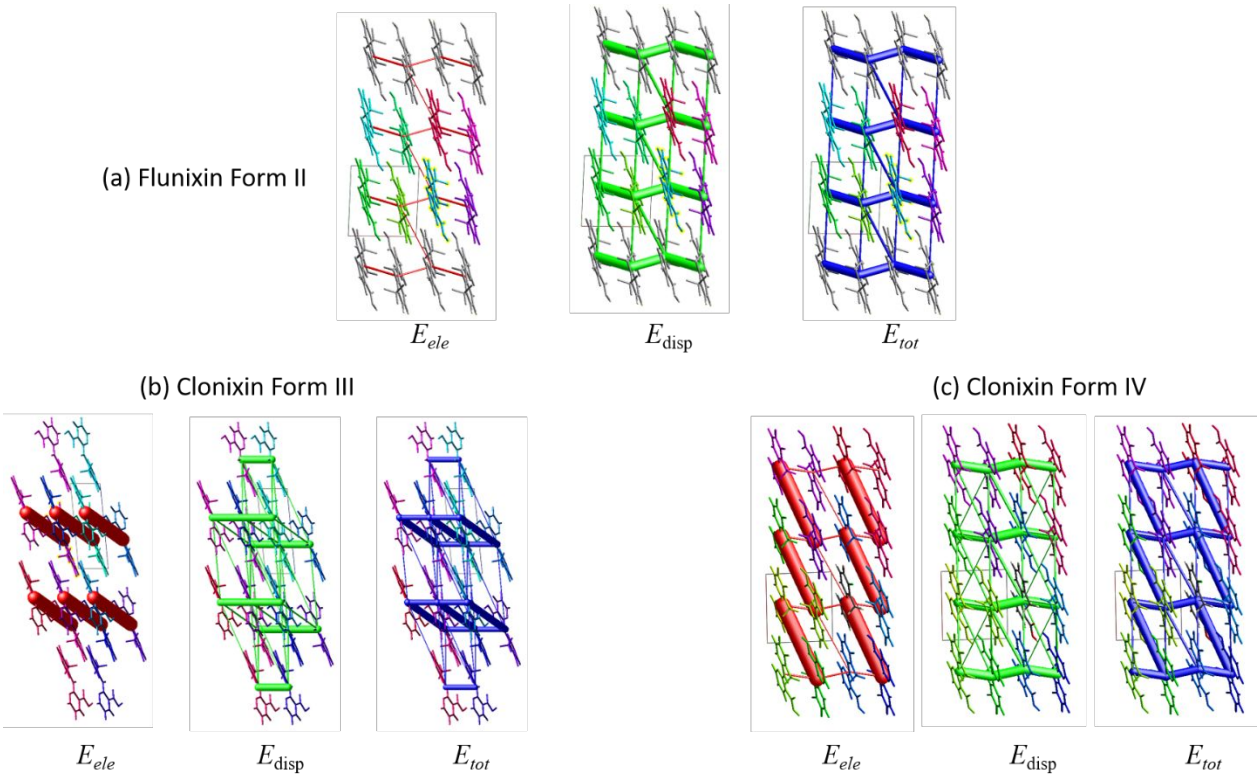

Figure 13. Energy frameworks for a) Flunixin Form II viewed down the ***c***-axis, b) Clonixin Form III down the ***a***-axis, and Clonixin Form IV down the ***c***-axis. The cylinder radii was scaled to 75 arbitrary units and the energy cutoff is 5 kJ mol^{-1}. E_{ele}, E_{disp}, and E_{tot} are represented in red, green, and blue, respectively.

Table 3. Summary of calculated energies (kJ mol^{-1}) for the polymorphs of Flunixin and Clonixin. (3.80 Å radius).

		E_{ele}	E_{pol}	E_{disp}	E_{rep}	E_{tot}
Flunixin	Form I	-92.6	-23.6	-187.5	165.6	-176.3
	Form II	-142.2	-32.3	-251.3	237.6	-246.4
Clonixin	Form I	-98.1	-24.7	-192.3	184.7	-175.4
	Form II	-65.9	-61.9	-149.2	146.6	-154.7
	Form III	-143.7	-35.1	-210.9	248.4	-208.6
	Form IV	-142.8	-33.8	-277.8	260.9	-256.5

Flunixin:Meglumine		-42.8	-13.7	-52.7	75.5	-54.7

Energy Model	k_{ele}	k_{pol}	k_{disp}	k_{rep}
CE-B3LYP ... B3LYP/6-31G(d,p) electron densities	1.057	0.740	0.871	0.618

CONCLUSIONS

Two polymorphs of the NSAID flunixin were prepared and characterized by ATR-FTIR and TGA/DSC analysis. Their structures, determined from powder and single crystal X ray diffraction, indicate very different conformations which lead to different hydrogen bonding patterns and different intermolecular interactions. The Hydrogen Bond Propensity calculation predicts the two polymorphs of flunixin and points to the possible existence of more polymorphs. The Hirshfeld surface analysis and energy framework calculations show the differences between the two polymorphs of flunixin and their respective similarities with polymorphs of the related NSAID clonixin. In particular, energy framework calculations demonstrated to be useful in distinguishing small differences in the crystalline packing that allowed to correctly classify the flunixin polymorphs. Crystallization experiments are underway to optimize the yield of polymorph II and to obtain other possible polymorphs of flunixin, in particular a zwitterionic form.

EXPERIMENTAL

1. Materials

Flunixin-meglumine raw material (FM-RM) was supplied by Laboratorios Reveex, Maracay, Venezuela. Concentrated HNO_3, acetone, ethanol, and hexane, purchased from different vendors, were used without further purification.

2. Separation and crystallization of flunixin

Flunixin powder (FP) was separated from the flunixin-meglumine raw material (FM-RM) by potentiometric titration of a 0.05 M solution of flunixin-meglumine (FM) (2.458 g of FM dissolved in 100 mL of water, pH = 8.515) with a 0.05 M solution of HNO_3 (0.35 mL of HNO_3 65% dissolved in 100 mL of water). The solution was kept under constant stirring and the nitric acid solution was added slowly from a burette while measuring the pH with a Crimson Basic 20 pH-meter calibrated with pH = 7 and pH = 4 buffer solutions (Laboratorio de Análisis Instrumental, Universidad de Los Andes, Mérida, Venezuela). The temperature in the laboratory was 22 °C. After adding about 1 mL of the acid solution (pH = 7.05) a white precipitate formed. This precipitate was later filtered by gravity and allowed to dry at room temperature for 12 hours. The remaining solution was allowed to evaporate slowly at ambient temperature.

Crystallization experiments were carried out using 50 mg of the precipitated flunixin in 1.5 mL of ethanol, acetone, and acetone-hexane 1:1 solution in 2 mL Eppendorf® Safe-Lock microcentrifuge tubes. Transparent prismatic crystals were obtained from ethanol and acetone solutions while transparent needles (along with prisms similar to those obtained from ethanol and acetone) grew in the acetone-hexane solution (see Figure SI-1). Based on powder and single crystal X ray diffraction studies performed on the materials, the separated flunixin and the prismatic crystals (from either acetone or ethanol) were labeled form I (F-I) and the needles (from acetone/hexane) were labeled form II (F-II).

3. Infrared Spectroscopy and thermal analysis

ATR-FTIR spectra for FM-RM, the separated flunixin (FP), and recrystallized flunixin (both forms, F-I and F-II) were recorded from 4000 to 500 cm^{-1}, in 24 scans, collected in 30 seconds, with a resolution of 4 cm^{-1}. The instrument used was a Bruker Alpha spectrophotometer with an ATR eco ZnSe accessory, located at Laboratorio de Química Orgánica y Biomolecular (LQOBio), Universidad Industrial de Santander, Bucaramanga, Colombia.

TGA and DSC analyses were carried out using a NETZSCH STA 449F5 instrument under dynamic nitrogen atmosphere at 50.0 mL min^{-1}. The instrument was allowed to equilibrate at 28.00 °C and

a heating ramp of 10.00 °C min^{-1} was applied up to 450.00 °C. The data was analyzed with the NETZSCH Proteus Thermal Analysis Version 6.1.0 software.

4. Characterization by X ray powder diffraction. Structure determination and refinement of Flunixin Form I from Powder Diffraction data.

Powder diffraction patterns for FM-RM and for FP were recorded on a Siemens D5005 diffractometer operating at 40kV/30mA, with CuKα radiation (λ= 1.5418 Å), and slits of 0.02 mm. The materials were gently ground in an agate mortar and dusted on top of a zero-background holder. Data were collected from 5° to 45° (2θ) in steps of 0.02° at 120 seconds per step. The high quality of the pattern of the separated flunixin allowed the structure determination of this material, prior to the single crystal study, using the programs DICVOL14,[28] TALP,[29] and GSAS-II,[30] as detailed in Section SI-3 of the Supporting Information. The powder diffraction data has been incorporated as entry PDF 00-068-1378 (as a Star-Quality pattern) in the Powder Diffraction File of the International Centre for Diffraction Data (ICDD).[8]

5. Single crystal X ray diffraction

Single crystal X ray diffraction data were collected at 293 K for Flunixin Forms I and II with a Rigaku XtaLAB P200 diffractometer operating at 50 kV and 40 mA. The diffractometer is equipped with a Pilatus 200K detector and SHINE (curved graphite monochromator) optics. MoKα radiation (λ=0.71075 Å) was used. CrystalClear[31] and CrysAlis Pro[32] were used for data collection, unit cell determination and refinement, integration, and reduction. Low temperature (100 K) data for Flunixin Form I was collected at Northwestern University using a Bruker APEX-II CCD Kappa Duo diffractometer, with MoKα radiation (λ = 0.71075 Å). Unit cell determination and refinement and data reduction were accomplished with Bruker APEX2[33] and Bruker SAINT[34] software. SHELXT[35] and SHELXL[36] implemented in shelXle[37] were used, respectively, for structure determination and refinement by full matrix least-squares. Diamond 3.0[38] was used for graphics. PLATON[24] was used for structure validation and geometrical calculations and enCIFer[39] for CIF editing. Additional details are provided in the Supporting Information, Section SI-4.

6. Hirshfeld Surface analysis and Energy Frameworks calculations.

Hirshfeld surface (HS) analysis was accomplished with CrystalExplorer17.[27] "Fingerprint plots" of d_e vs. d_i were obtained for the two polymorphs of flunixin and for the four polymorphs of clonixin. For flunixin, d_{norm} values[26] were mapped onto the HS in the range -0.80 to 1.70 to aid the visualization of intermolecular contacts. Details are provided in Section SI-6 of the Supporting Information. Section SI-7 describes the calculation of Energy frameworks using CrystalExplorer17[27] and the scaling procedures employed.[40-41]

CRYSTALLOGRAPHIC DATA

Single crystal data for flunixin Form I (Ambient Temperature and Low Temperature) and Form II have been deposited with the Cambridge Crystallographic Data Centre under deposition numbers 1827219, 1884640, and 1884673, respectively. They can be accessed free of charge at https://www.ccdc.cam.ac.uk/structures. Powder diffraction data for flunixin Form I has been deposited with the International Centre for Diffraction Data (ICDD) as entry PDF 00-068-1378.

ASSOCIATED CONTENT

Supporting Information. Additional information noted in text is available free of charge via the ACS publications site http://pubs.acs.org. Sections SI-1 to SI-7 contain ATR-FTIR spectra, TGA/DSC curves, details of the structure determination and refinement by powder data, details of single crystal data collection, details of Hydrogen Bond Propensity, Hirshfeld Surface analysis and Energy Frameworks calculations. Figures SI-1 to SI-12 and Tables SI-1 to SI-13 as well as References for the experimental procedures are included.

AUTHOR INFORMATION

Corresponding Author

*E-mail: gdiazdedelgado@gmail.com / diaz@ula.ve

ACKNOWLEDGEMENTS

We dedicate this contribution to Dr. William Jones on the occasion of his retirement, in appreciation for his contributions to the understanding of the solid-state chemistry of pharmaceutical compounds.

The authors thank Lic. M. A. Ramírez and Lic. A. G. Mora (ULA) and Qco. C. Alvarez (UIS) for technical assistance, and Lic. J. J. Dávila of Laboratorios Reveex, Venezuela. Thanks are also due to Charlotte Stern (Northwestern U., USA) for data collection at low temperature of Form I, during the 2017 ACA Summer Course in Chemical Crystallography and to Dr. Amy Sarjeant (CCDC) for fruitful discussions regarding Hydrogen Bond Propensities. This work was supported in part by Vicerrectoría de Investigación y Extensión, Universidad Industrial de Santander (UIS), Colombia. Access to the *Cambridge Structural Database* (CSD) for Universidad de Los Andes (Venezuela) was possible through the *Frank H. Allen International Research & Education Programme* (FAIRE) from the *Cambridge Crystallographic Data Centre* (CCDC).

REFERENCES

(1) Brunton, L. L.; Lazo, J. S.; Parker, K. L., *Goodman & Gilman's: The Pharmacological Basis of Therapeutics*. 11 ed.; McGraw-Hill Medical Publishing Division: New York, NY, 2006; p 2021.

(2) http://clincalc.com/DrugStats/Drugs/Diclofenac Access date: December 19, 2018

(3) Jaussaud, P. La Flunixine et son utilisation chez le cheval. *Ann. Rech. Vét.* **1986,** *17*, 353-362.

(4) Cao, X.-J.; Sun, C.-R.; Pan, Y.-J. The complex of flunixin and meglumine. *Acta Crystallogr., Sect. E* **2003,** *59*, o1471-o1473.

(5) Fédération Equestre Internationale, F., Equine Prohibited Substances Database. Fédération Equestre Internationale: Lausanne, Switzerland, 2010-2018. http://prohibitedsubstancesdatabase.feicleansport.org/.

(6) USP Veterinary Pharmaceutical Information Monographs - Anti-inflammatories. *J. Vet. Pharmacol. Therap.* **2004,** *27*, 1-110.

(7) Groom, C. R.; Bruno, I. J.; Lightfoot, M. P.; Ward, S. C. The Cambridge Structural Database. *Acta Crystallogr., Sect. B* **2016,** *72*, 171-179.

(8) Kabekkodu, S. *PDF-4/Organics Database*. International Centre for Diffraction Data (ICDD): Newtown Square, PA, USA, 2015.

(9) Long, S.; Parkin, S.; Siegler, M.; Brock, C. P.; Cammers, A.; Li, T. Polymorphism of an Organic System Effected by the Directionality of Hydrogen-Bonding Chains. *Cryst. Growth Des.* **2008,** *8*, 3137-3140.

(10) Long, S.; Parkin, S.; Siegler, M. A.; Cammers, A.; Li, T. Polymorphism and Phase Behaviors of 2-(Phenylamino)nicotinic Acid. *Cryst. Growth Des.* **2008,** *8*, 4006-4013.

(11) Long, S.; Li, T. Controlled Formation of the Acid−Pyridine Heterosynthon over the Acid−Acid Homosynthon in 2-Anilinonicotinic Acids. *Cryst. Growth Des.* **2009,** *9*, 4993-4997.

(12) Long, S.; Li, T. Enforcing Molecule's π-Conjugation and Consequent Formation of the Acid−Acid Homosynthon over the Acid−Pyridine Heterosynthon in 2-Anilinonicotinic Acids. *Cryst. Growth Des.* **2010,** *10*, 2465-2469.

(13) Long, S.; Siegler, M. A.; Mattei, A.; Li, T. Phase Transition from Two $Z' = 1$ Forms to a $Z' = 2$ Form of a Concomitant Conformational Polymorphic System. *Cryst. Growth Des.* **2011,** *11*, 414-421.

(14) Lee, E. H.; Boerrigter, S. X. M.; Rumondor, A. C. F.; Chamarthy, S. P.; Byrn, S. R. Formation and Solid-State Characterization of a Salt-Induced Metastable Polymorph of Flufenamic Acid. *Cryst. Growth Des.* **2008,** *8*, 91-97.

(15) Nath, N. K.; Kumar, S. S.; Nangia, A. Neutral and Zwitterionic Polymorphs of 2-(p-Tolylamino)nicotinic Acid. *Cryst. Growth Des.* **2011,** *11*, 4594-4605.

(16) Kumar, S. S.; Nangia, A. A Solubility Comparison of Neutral and Zwitterionic Polymorphs. *Cryst. Growth Des.* **2014,** *14*, 1865-1881.

(17) Takasuka, M.; Nakai, H.; Shiro, M. Infrared spectral and X-ray studies of polymorphic forms

of 2-(2-methyl-3-chloroanilino)nicotinic acid. *J. Chem. Soc., Perkin Trans. 2* **1982,** 1061-1067.

(18) Macrae, C. F.; Bruno, I. J.; Chisholm, J. A.; Edgington, P. R.; McCabe, P.; Pidcock, E.; Rodriguez-Monge, L.; Taylor, R.; van de Streek, J.; Wood, P. A. Mercury CSD 2.0– new features for the visualization and investigation of crystal structures. *J. Appl. Crystallogr.* **2008,** *41*, 466-470.

(19) Nauha, E.; Bernstein, J. "Predicting" Crystal Forms of Pharmaceuticals Using Hydrogen Bond Propensities: Two Test Cases. *Cryst. Growth Des.* **2014,** *14*, 4364-4370.

(20) Galek, P. T. A.; Fábián, L.; Motherwell, W. D. S.; Allen, F. H.; Feeder, N. Knowledge-based model of hydrogen-bonding propensity in organic crystals. *Acta Crystallogr. Sect. B* **2007,** *63*, 768-782.

(21) Galek, P. T. A.; Allen, F. H.; Fabian, L.; Feeder, N. Knowledge-based H-bond prediction to aid experimental polymorph screening. *CrystEngComm* **2009,** *11*, 2634-2639.

(22) Bruno, I. J.; Cole, J. C.; Kessler, M.; Luo, J.; Motherwell, W. D. S.; Purkis, L. H.; Smith, B. R.; Taylor, R.; Cooper, R. I.; Harris, S. E.; Orpen, A. G. Retrieval of Crystallographically-Derived Molecular Geometry Information. *J. Chem. Inf. Comp. Sci.* **2004,** *44*, 2133-2144.

(23) Etter, M. C.; MacDonald, J. C.; Bernstein, J. Graph-set analysis of hydrogen-bond patterns in organic crystals. *Acta Crystallogr., Sect. B* **1990,** *46*, 256-262.

(24) Spek, A. L. Structure validation in chemical crystallography. *Acta Crystallogr., Sect. D* **2009,** *65*, 148-55.

(25) Krishna Murthy, H. M.; Vijayan, M., 2{[3-(Trifluoromethyl)phenyl]amino}-3-pyridinecarboxylic acid (niflumic acid). *Acta Crystallogr. Sect. B* **1979,** *35*, 262-263.

(26) Spackman, M. A.; Jayatilaka, D. Hirshfeld surface analysis. *CrystEngComm* **2009**, *11*, 19-32.

(27) Turner, M. J.; McKinnon, J. J.; Wolff, S. K.; Grimwood, D. J.; Spackman, P. R.; Jayatilaka, D.; Spackman, M. A. CrystalExplorer17; University of Western Australia: Crawley, Australia, 2017. http://hirshfeldsurface.net.

(28) Boultif, A.; Louer, D. Powder pattern indexing with the dichotomy method. *J. Appl. Crystallogr.* **2004,** *37*, 724-731.

(29) Vallcorba, O.; Rius, J.; Frontera, C.; Miravitlles, C. TALP: a multisolution direct-space strategy for solving molecular crystals from powder diffraction data based on restrained least

squares. *J. Appl. Crystallogr.* **2012,** *45*, 1270-1277.

(30) Toby, B. H.; Von Dreele, R. B. GSAS-II: the genesis of a modern open-source all purpose crystallography software package. *J. Appl. Crystallogr.* **2013,** *46*, 544-549.

(31) Rigaku *CrystalClear-SM Expert*, 2.1 b45; Rigaku: Rigaku Americas, The Woodlands, TX, USA, and Rigaku Corporation, Tokyo, Japan., 2015.

(32) RigakuOxfordDiffraction *CrysAlisPro Software system*, 171.39.28e; Rigaku Corporation: Oxford, UK, 2015.

(33) Bruker *APEX2*, Bruker AXS Inc.: Madison, Wisconsin, USA, 2012.

(34) Bruker *SAINT*, Bruker AXS Inc.: Madison, Wisconsin, USA, 2012.

(35) Sheldrick, G. M. SHELXT - Integrated space-group and crystal-structure determination. *Acta Crystallogr., Sect. A* **2015,** *71*, 3-8.

(36) Sheldrick, G. M. Crystal structure refinement with SHELXL. *Acta Crystallogr., Sect. C* **2015,** *71*, 3-8.

(37) Hubschle, C. B.; Sheldrick, G. M.; Dittrich, B. ShelXle: a Qt graphical user interface for SHELXL. *J. Appl. Crystallogr.* **2011,** *44*, 1281-1284.

(38) Brandenburg, K. *DIAMOND*, 3.0; Crystal Impact GbR: Bonn, Germany, 1999.

(39) Allen, F. H.; Johnson, O.; Shields, G. P.; Smith, B. R.; Towler, M. CIF applications. XV. enCIFer: a program for viewing, editing and visualizing CIFs. *J. Appl. Crystallogr.* **2004,** *37* (2), 335-338.

(40) Mackenzie, C. F.; Spackman, P. R.; Jayatilaka, D.; Spackman, M. A. CrystalExplorer model energies and energy frameworks: extension to metal coordination compounds, organic salts, solvates and open-shell systems. *IUCrJ* **2017,** *4*, 575–587.

(41) Edwards, A. J.; Mackenzie, C. F.; Spackman, P. R.; Jayatilaka, D.; Spackman, M. A. Intermolecular interactions in molecular crystals: what's in a name?. *Faraday Discuss.* **2017,** *203*, 93–112.

For Table of Contents Use Only

Polymorphism in the anti-inflammatory drug Flunixin and its relationship with Clonixin.

María Cecilia Dávila-Miliani[1], Analio Dugarte-Dugarte[1], Robert A. Toro[2], Jines E. Contreras[1], Hernando A. Camargo[3], José Antonio Henao[2], José Miguel Delgado[1], Graciela Díaz de Delgado[1]

[1]Laboratorio de Cristalografía-LNDRX, Departamento de Química, Facultad de Ciencias, Universidad de los Andes, Mérida 5101, Venezuela.
[2]Grupo de Investigación en Química Estructural (GIQUE), Escuela de Química, Universidad Industrial de Santander, Bucaramanga, Colombia.
[3]Grupo de Investigación en Nuevos Materiales y Energías Alternativas, Facultad de Química Ambiental, Universidad Santo Tomás, Florida Blanca, Colombia.

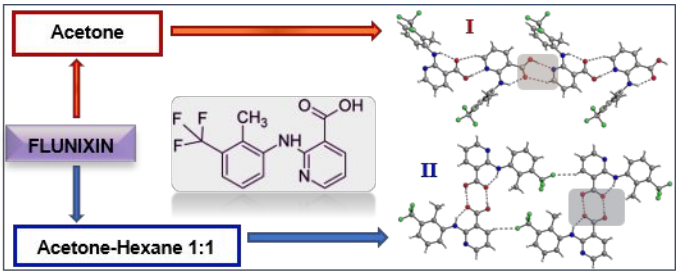

Synopsis. Two conformational polymorphs of the non-steroidal anti-inflammatory drug flunixin were grown and characterized by ATR-FTIR, TGA/DSC, and powder and single crystal X ray diffraction. Form I exhibits intermolecular hydrogen bonds based on the acid—pyridine heterosynthon while Form II displays the acid—acid homosynthon.